International Journal of Engineering &Technology, 13 (2) (2024) 194-203

International Journal of Engineering & Technology

Website: www.sciencepubco.com/index.php/IJET

Research paper

Modelling of improved LSTM +1D convolution neural network methods for the diagnosis of SKF bearings

Signe Feudjeu Josias Éric [1]*, Nzié Wolfgang [1, 2], Ngnassi Djami Aslain Brisco [2], Ntsama Eloundou Pascal [3], Chassem Priva [4]

[1] Department of Mechanical Engineering, National School of Agro-Industrial Sciences, University of Ngaoundéré, Ngaoundéré, Came-roon
[2] Department of fundamental Sciences and Technique of Engineer, Chemical Engineering and Mineral Industries School, University of Ngaoundéré, Ngaoundéré, Cameroon
[3] Department of Physics, Higher Teacher Training College, University of Bertoua, Bertoua, Cameroon
[4] Department of Mathematics and Computer Sciences, Faculty of Sciences, University of Dschang, Dschang, Cameroon
**Corresponding author E-mail: josiassigne@gmail.com*

Abstract

The ability to accurately detect and predict faults in automotive bearings is essential for diagnostic applications in the maintenance process. Although previous methods can accurately identify the various faults on bearings, they mostly produce erroneous results in the presence of certain mechanical factors when classifying the data. We propose a new diagnostic framework based on one-dimensional convolutional neural network (CONV1D) modelling and improved long short-term memory (LSTM), together with confusion matrices to evaluate data classification using the Deep Learning algorithm. Our framework classifies the data by taking into account the mechanical factors of the bearings (sudden load, rotation speed, operating temperature, etc.). Our results improve the training accuracy of the model to over 96.6%, with a percentage error of 23.29% for 50 iterations (repetitions). This percentage of training accuracy could be closer to 100% and that of the error margins to 0% if we increase the number of iterations. These results underline the promise of our method across our model and indicate how future expansion of the model by combining three methods can lead to further improvements in training accuracy with fewer errors and fewer iterations.

Keywords: *Modeling; Diagnostics; Convolutional Neural Networks; LSTM.*

1. Introduction

Bearings are essential components in mechanisms such as those used in cars, to ensure that they are guided in rotation. Bearing faults are the main source of problems with the coaxiality of automotive transmission shafts and the noise they produce. The various conventional, scientific methods of diagnosing bearings used in the past have so far produced erroneous results. This drew the attention of several researchers and led them to propose more innovative diagnostic methods. For example, Gu et al. [1] proposed a method combining LSTM and discrete wavelet transform to diagnose ball defects in multi-sensor bearings. However, this method takes too long to learn, especially when the size of the fault is large. Oh et al. [2] designed a multiscale convolutional recurrent neural network for detection of bearing faults in high-noise manufacturing environments. However, this method does not detect subdivided and internal defects and does not completely suppress noise. Zhao et al. [3] proposed a regularised LSTM memory method for predicting the remaining service life of induction motor bearings using the PRONOSTIA platform. However, the learning algorithm implemented by this method does not take into account mechanical factors on the bearings. Khorram et al. [4] developed a deep learning approach by combining CNN+LSTM end-to-end for bearing fault diagnosis based on accelerometers. The model in this approach can diagnose with a very large dataset but requires too much computation during the training process which consequently makes the model slow and requires a machine with good computing power to produce reliable results. Qiao et al. [5] design a deep recurrent convolutional neural network with LSTM memory for bearing fault diagnosis under high noise and variable load conditions. This method is more suitable for diagnosing bearing faults in the event of noise and load interference, except that the training accuracy of the model cannot exceed 75% when the noise increases and can be as high as 95% under slight noise. The contributions of this paper are improvements on the work mentioned above, which consist in removing the limitations encountered in this work. These include: taking into account mechanical factors on the bearings in order to obtain a quality diagnosis, the possibility of the model training with a very large data set with a training and test time shorter than those mentioned in the other work already studied. All this will only be possible by proposing a method combining the one-dimensional CNN + the improved LSTM memory in order to improve the training percentages of the diagnostic model to over 96% with a considerably low margin of error.

This work is organized as follows: in the second section, we will talk about the generalities on SKF bearings and their defects in order to describe the classification techniques for a good diagnosis, then in the third section, we will present
the material and the methods that allow to identify the source of the data, the methods and the parameters of the proposed model and finally, describe the proposed model. In section four, we will present the results of the experiments carried out and the discussions, and finally in section five, we will give the conclusion and the prospects for the continuation of the work.

2. General information about bearings

2.1. Introduction to bearings

Bearings are components fitted in a mechanism to transmit forces and ensure shaft rotation. In other words, they guide the shaft in rotation. Bearings are made up of two concentric steel rings, called the inner ring and outer ring, with raceways (surfaces on which the rolling elements "roll"), rolling elements, balls or rollers, generally made of steel, allowing the two rings to move with minimal friction, and a cage separating and guiding the rolling elements. The bearing consists of four components: outer race, inner race, ball, and cage, as shown in Figure 1 (Slavic et al. [6]).

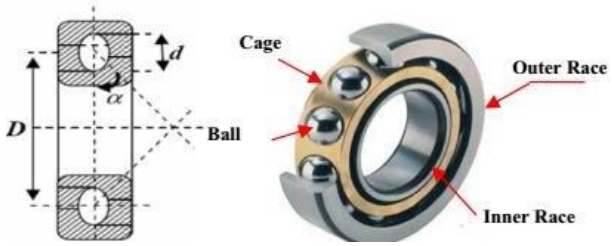

Fig. 1: Components of Bearing.

2.2. Bearing faults

2.2.1. Inner ring defect

This is characterized by the presence of a line at the characteristic frequency of the fault (fd,bi). This frequency is modulated by the rotation frequency (side bands around the fault line (Amar Chiter [7]) (see equation 1):

$$fdbi = \frac{fr.Nb}{2}\left(1+\left(\frac{Db}{Dm}\cos(\alpha)\right)\right) \quad (1)$$

With fr: rotation frequency; α: contact angle; Dm: mean bearing diameter; Db: ball diameter and Nb: number of balls.
Figures 2 and 3 give the theoretical images of this defect (radial and axial loads).

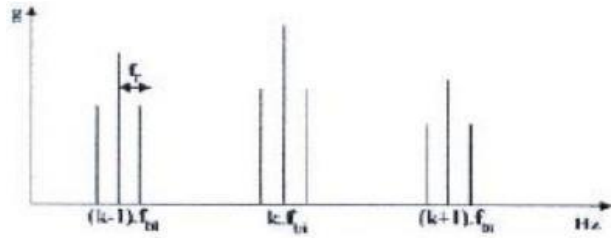

Fig. 2: Spalling on the Inner Ring (Radial Load).

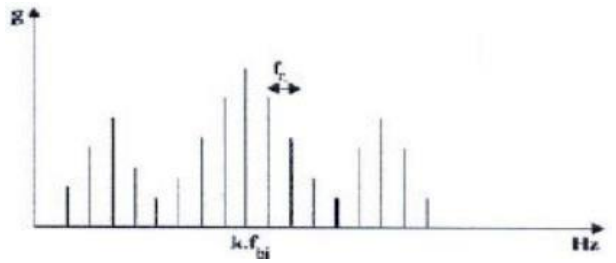

Fig. 3: Spalling on the Inner Ring (Axial Load).

2.2.2. Outer ring defect

This fault is characterized by the presence of a line at frequency (fd, be) (see equation 2). Although the load applied to the outer ring is constant, there is an amplitude modulation at the shaft rotation frequency around the fault frequency.

$$fdbe = \frac{fr.Nb}{2}\left(1-\left(\frac{Db}{Dm}\cos(\alpha)\right)\right) \quad (2)$$

Figures 4 and 5 gives the theoretical spalling images and the real spalling spectrum, all characteristics of the defect on the outer ring, respectively.

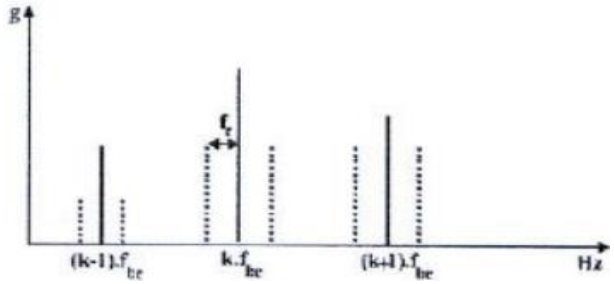

Fig. 4: Spalling on the Inner Ring.

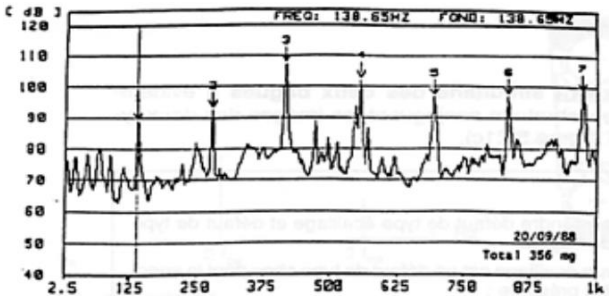

Fig. 5: Spalling on the Outer Ring.

2.2.3. Rolling element fault

The first characteristic fault frequency corresponds to the frequency of rotation of the rolling element on itself (see equation 3). In addition, this rolling element encounters the inner ring once and the outer ring once per revolution, so it generates shocks at twice this frequency.

$$fball = \frac{fr.Dm}{2.Db}\left(1-\left(\frac{Db}{Dm}\cos(\alpha)\right)\right) \tag{3}$$

Figure 6 gives the theoretical image of spalling on the balls.

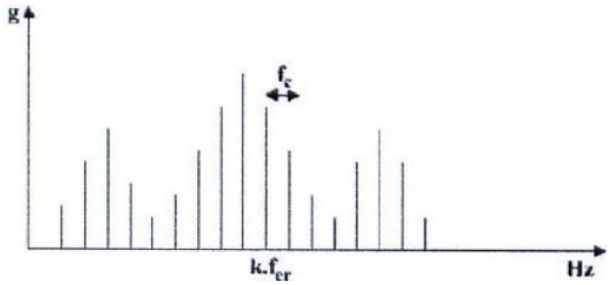

Fig. 6: Spalling on the Rolling Element.

2.2.4. Cage fault

This is characterized by the presence of a line at the characteristic frequency of the fault (fc). The frequency at which a passing fault occurs is given by the equation 4.

$$fc = \frac{fr}{2}\left(1-\left(\frac{Db}{Dm}\cos(\alpha)\right)\right) \tag{4}$$

2.3. Detecting bearing faults

In order to detect bearing faults, it is necessary to be able to classify observable situations as normal or abnormal. This classification is not trivial in the case of bearings, given the sheer volume of drive data. Abnormal situations are considered as failed states or faults.
Classification technique is based on deep learning (DL) algorithms for convolutional neural networks. This algorithm is more compatible with larger amounts of training data. As the amount of data increases, the performance of DL can significantly outperform most Most Learning (ML) algorithms (Schmidhuber [8]). Figure 7 shows the performance of deep learning over most learning as a function of the amount of data.

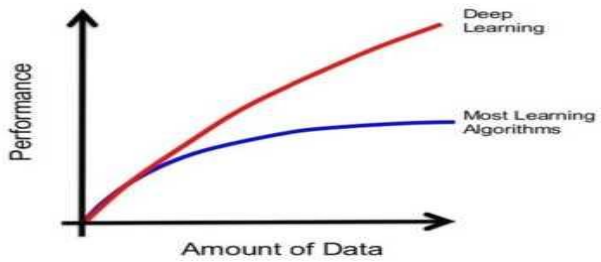

Fig. 7: Comparison of the Performance of the DL Algorithm with Conventional Learning Algorithms (ML).

Once the data has been classified by the DL algorithm, evaluation approaches must be used to show whether the model learning algorithm manages to classify correctly. These evaluation approaches are none other than confusion matrices.

3. Materials and methods

3.1. Data collection bench

To achieve better diagnosis by convolutional networks combined with the improved LSTM network, we resorted to Online SKF bearing data from the Case Western Reserve University (CWRU) laboratory data collection rig based in the USA already collected and contained in their data bank. The bench has a sampling rate of 48KHz, with a sampling time of 10s for each data point, the shaft speed is 1725rpm, producing 1670 data points collected for one revolution. This bench presented in Figure 8 develops an output power of 2.2 Kw. In addition, we used the Jupiter notebook of the ANACONDA software, which was of fundamental importance for the training process, testing and validation of the results (Pan et al. [8]).

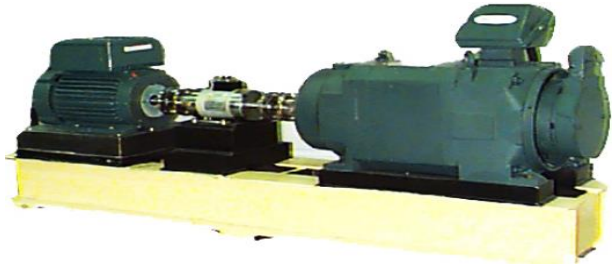

Fig. 8: Test Bench at Case Western Reserve University (CWRU): USA.

3.2. Working methods

3.2.1. Diagnostic methods using convolutional neural networks (CNN)

a) Definition and structure of CNS

Diagnostic technique using dynamic monitoring by convolutional neural networks are based on the existence of a learning database and not on the existence of a formal or functional model of the equipment.

An CNN as described in Figure 9 by its structure is basically an ANN (Artificial Neural Network) with a different architecture but retaining the characteristics of a classic ANN, which has the particularity of filtering the input data before processing and processing the data in the form of a table, an image or speech (Fukushima [10]). This is because the data we have obtained on online bearings is in the form of a table with rows and columns of very large volume. The structure of this type of neural network is as follows:

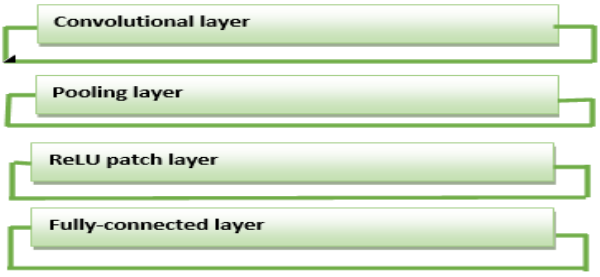

Fig. 9: Structure of a Convolutional Neural Network.

The convolution layer is the key component of convolutional neural networks. Its purpose is to identify the presence of a set of features (filters) in the data received as input for the pooling layer. The pooling operation consists of reducing the size of the data, while preserving its important characteristics, in order to make learning faster and more efficient and avoid over-learning. The ReLU (Rectified Linear Units) correction layer therefore replaces all negative input values with zeros. It acts as an activation function. The final fully-connected layer is used to classify the input data to the network: it returns a vector of size N, where N is the number of classes in our data classification problem.

b) CNN architecture

The architecture of the CNN model based on fault diagnosis presented in Figure 10 is made up of several filters to select the data properly in order to avoid overlearning as much as possible, since this type of CNN always works with a very large volume of data, otherwise learning will not be optimal and effective. The structure of the CNN is as follows (Wen et al. [11]).

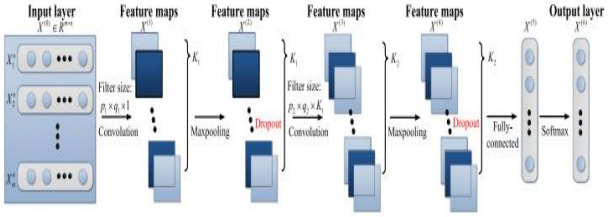

Fig. 10: Example of the Architecture of A CNN (CONV1D) Based on A Fault Diagnosis Model.

3.2.2. Method using the LSTM network

The LSTM layer is used in this work to be able to read and process data in the form of vibration signals related to bearing faults (L Hochreiter and Schmidhuber [12]). To exploit these signals with the LSTM network, we can use vibration analysis methods such as: the time method, the frequency method (spectral analysis) and also the time-frequency method. The structure of an LSTM network is shown in the Figure 11.

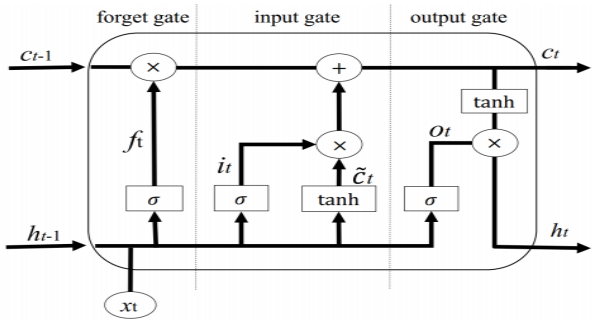

Fig. 11: Structure of an LSTM Network.

ft represents the calculation gates corresponding to the previous points in the neural network. And is given by the equation 5.

$$ft = \sigma\left(w_{ft} z_t + w_{hf} h_{ht-1} + b_f\right) \tag{5}$$

σ is the sigmoid function, w are the weights, z_t is the current input and b_f represents the biases.

3.3. Model

3.3.1. Tables describing the data and parameters characteristic of the model

According to Table1 below, we have 10 data sets corresponding to ten bearing states, i.e. one normal state and nine fault states. Each dataset contains 290 samples from which 240 are randomly selected to drive the network and the remaining 50 to test the network. This table is broken down as follows:

Table1: Characteristic Data of the Then Bearing States Required for Diagnosis by Our Final Model

Bearing condition	Fault size	Drive data	Test data	Class characters
Normal	-	240	50	0
Fault 1 on the ball	0.18	240	50	1
Fault 2 on the ball	0.36	240	50	2
Fault 3 on the ball	0.53	240	50	3
Inner ring fault 1	0.18	240	50	4
Inner ring fault 2	0.36	240	50	5
Inner ring fault 3	0.53	240	50	6
Fault 1 on outer ring	0.18	240	50	7
Fault 2 on outer ring	0.36	240	50	8
Fault 3 on outer ring	0.53	240	50	9

Looking at Table 2 below, we've defined the parameters for each layer of our network.

Table2: Characteristic Parameters of the Final Model

Layers	Type	Parameters of layers	Others parameters
1	Input layer	Dimension = [2400, 80,20]	Maximum number of iterations = 50
2	Convolution layer	KC = 20 ; KL = 64	Dropout = 29
3	Pooling layer	PL = 10	Activation = relu
4	LSTM layer	Number of units = 128	Classifier = softmax
5	Output layer	Output fields = 10	Optimizer = Adams

For example, the input layer has a dimension of [2400, 80,20], i.e. we have 2400 data samples, so each sample is represented in an array of 80 rows and 20 columns. However, for the convolution layer, we have the KC (kernel channel) which is the vector field of our convolution layer, and the KL (kernel length) which corresponds to the length of the vector in this layer. And the LSTM layer, which reads and processes the 10 signals corresponding to the 10 bearing states shown in Table 1. The parameters mentioned in Table 2 are presented in our RNC training software in a more detailed form as can be seen in Figure 12 below.

Layer (type)	Output Shape	Param #
conv1d_27 (Conv1D)	(None, 80, 32)	40992
max_pooling1d_26 (MaxPooling	(None, 40, 32)	0
conv1d_28 (Conv1D)	(None, 40, 64)	262208
max_pooling1d_27 (MaxPooling	(None, 20, 64)	0
conv1d_29 (Conv1D)	(None, 20, 64)	524352
max_pooling1d_28 (MaxPooling	(None, 10, 64)	0
time_distributed_13 (TimeDis	(None, 10, 64)	0
lstm_25 (LSTM)	(None, 10, 32)	12416
dropout_27 (Dropout)	(None, 10, 32)	0
lstm_26 (LSTM)	(None, 10, 64)	24832
dropout_28 (Dropout)	(None, 10, 64)	0
lstm_27 (LSTM)	(None, 128)	98816
dropout_29 (Dropout)	(None, 128)	0
dense_41 (Dense)	(None, 60)	7740
dense_42 (Dense)	(None, 50)	3050

Fig. 12: Representation of the Parameters of Each Layer of the Enhanced CNN and LSTM Networks Organized in the Programming Software.

The ten vibration signals used as data for the LSTM layers and corresponding to the 10 bearing states obtained using the accelerometer on the CRWU bearing experiment bench are those shown in Figure 15 below (Huang and Baddour [13]).

3.3.2. Model architecture

The architecture of our model shown in Figure 13 is illustrated in this form. The data obtained is processed to obtain a dataset that must be compatible with our learning algorithm. The algorithm generates an initial model from the training data, which is then combined with the test data to obtain a prediction of the diagnosis. This prediction is then evaluated. If it is good, we adopt the final model and if it is bad, we send back to the algorithm for further training until we obtain a good final model.

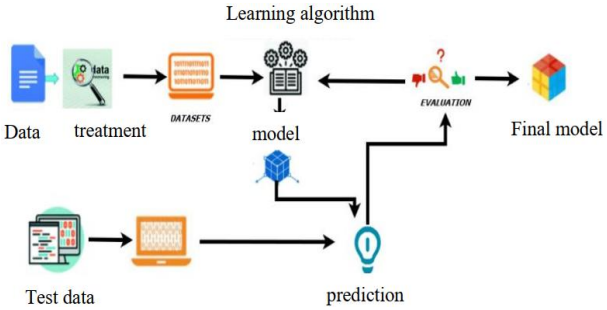

Fig. 13: Architecture of the Proposed Fault Diagnosis Model.

3.3.3. Final model

The model obtained, as summarized in the table above, contains an input layer, three convolution layers, each accompanied by a pooling layer, three LSTM layers, three fully connected layers, a dropout + flatten layer (one of which is used to set the percentage of data to be discarded and the other to flatten the data into signals in order to convert them into vectors for easier reading by the LSTM layers) and an output layer. This model is shown in Figure 14.

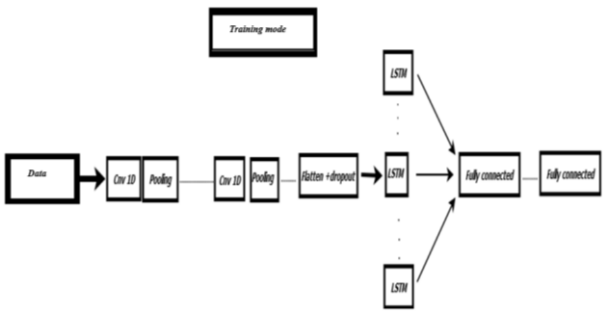

Fig. 14: CNN+LSTM Drive Model for Fault Diagnosis.

The vibration signals for the ten bearing fault states taken from the experimental bench at Case Western Reserve University (CWRU): USA, which enabled us to drive the LSTM network, are shown in Figure 15.

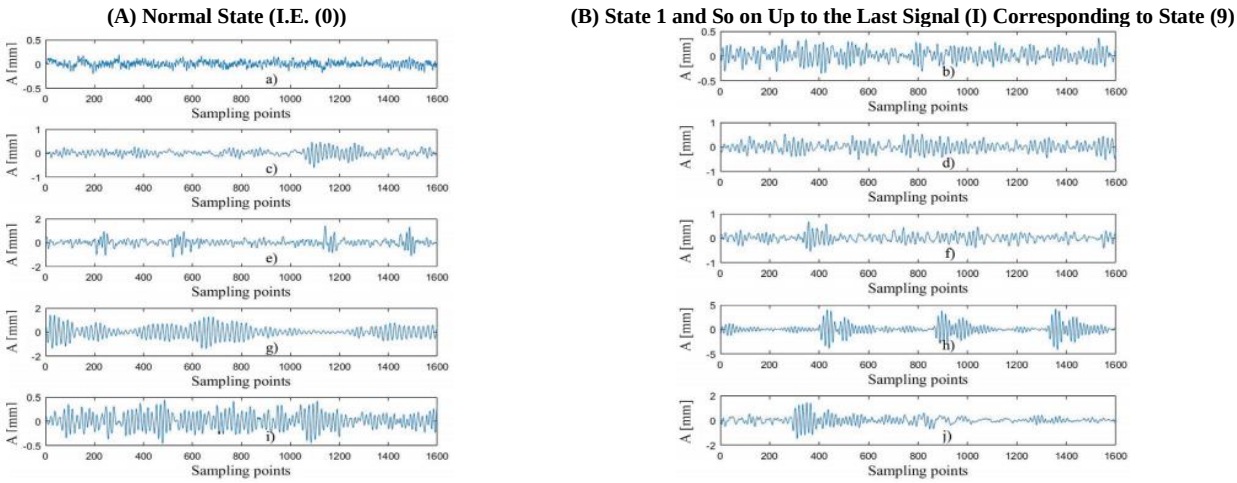

Fig. 15: Vibration Signals for the Ten Bearing States Used by the LSTM Network.

4. Experimentation and results

This section presents the behavior of our model when trained using data sets taken on-line from the CWRU's experimental bench and vibration signals from the same experimental bench. The model generates output results that enable us to assess its performance, or lack of it, in order to predict the quality of the diagnosis carried out on the bearings. We will first train the model by separating the data and then train the model by combining the data. The purpose of this is to evaluate the different margins of error and accuracy percentages for each case, in order to justify combining the two methods, which will highlight the limitations of using each method on its own. Given the volume of data, we will set the minimum number of iterations at 14 and the maximum at 50. The evaluation curves obtained are those presented in the rest of the paper.

4.1. Training and test accuracy evaluation curves for CONV1D layers

The programming language used to obtain all the result curves is (TensorFlow python) from the anaconda software. Figure 16 allows us to evaluate the training accuracy of the model only by the convolution layers for a test of 14 iterations in order to judge its performance in terms of percentage for a fairly short time.

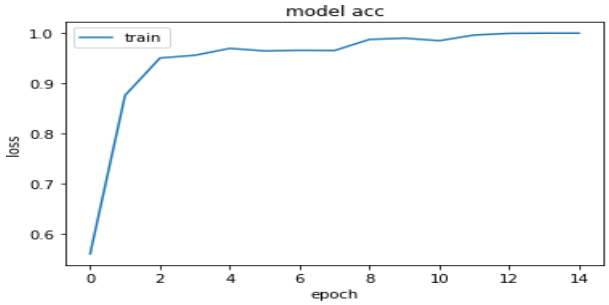

Fig. 16: Accuracy Rate of Model Training by CONV1D Layers Only for 14 Iterations.

The curve in Figure 16 above is the result of the first iteration of our model. It shows the training accuracy of the data from the improved one-dimensional convolution layers for 14 iterations only. The training accuracy in this case is 97% with a margin of error of 0.05. The curves of Figure 17 will give us slightly different results by increasing the number of iterations to 50.

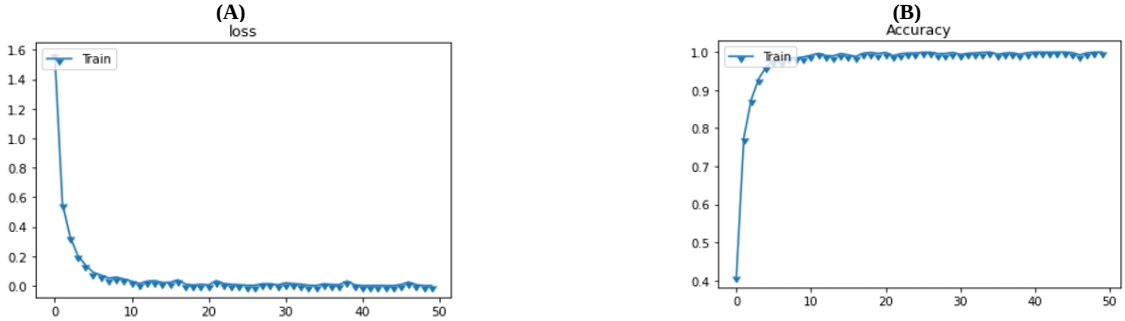

Fig. 17: Error Rate and Accuracy of Model Training Using CONV1D Layers for 50 Iterations.

The first curve (a) in Figure 17 shows the error rate using data collected and processed from Case Western Reserve University (CWRU) only. We notice that the curve is decreasing, which means that the training errors are tending towards zero, which increases the performance of the training, so there are fewer errors in the processing of the input data. Our curve gives us an error of 0.14. However, the second curve (b) shows us the accuracy of training the data to predict a good diagnosis. We can see that the accuracy tends towards 10, i.e. towards a percentage of 100%. Our curve gives us an accuracy of 98.5%.

4.2. Training and test accuracy evaluation curves for LSTM networks

The curves of Figure 18 allow to evaluate the training accuracy of the model only for the LSTM networks for a test of 40 iterations in order to judge its performance in terms of percentage also.

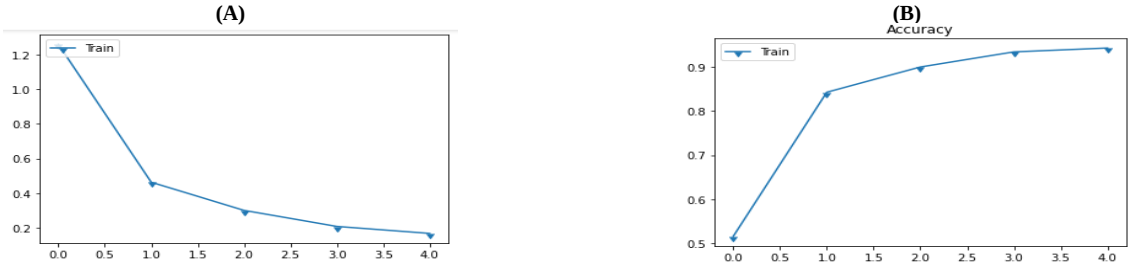

Fig. 18: Error Rate and Accuracy of Model Training by LSTM Networks for 40 Iterations.

The first curve (a) in Figure 18 shows the error rate using the vibration signal data for the ten rolling states only. We notice that the curve is decreasing, which means that the training errors are also tending towards zero, which increases the performance of the training, so there are fewer errors in the processing of the input data. Our curve gives us an error of 0.16. However, the second curve (b) shows us the accuracy of training the data to predict a correct diagnosis. Our curve gives us an accuracy of 94%.

4.3. Training and test accuracy evaluation curves for CONV1D+LSTM networks

The curves in Figure 19 give us the results of the fusion of the two methods, which allows us to see a clear improvement both in the training accuracy of the model and in the reduction of the margin of error.

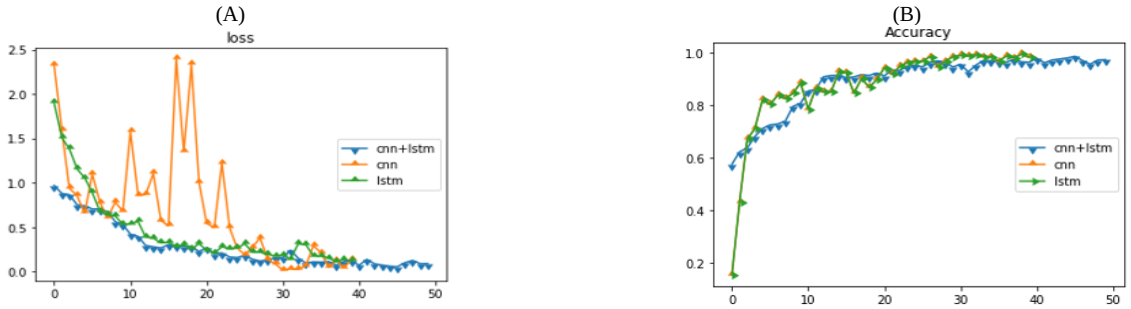

Fig. 19: CONV1D+LSTM Layer Combination for 50 Iterations.

The first curve (a) in Figure 19 shows the error rate using the data collected and processed from Case Western Reserve University (CWRU) and the vibration signal data from the ten rolling conditions. Our training error curve gives us a percentage error of 23.29% for 50 iterations with the two methods combined. This percentage could perhaps be improved, i.e. reduced, by increasing the number of iterations, but this would require more time. However, the second curve (b) shows us the accuracy of training the data to predict a good diagnosis. Our curve gives us an accuracy of 96.6%, slightly lower than that of the CONV1D curve and slightly higher than that of the LSTM curve. This accuracy could be improved by increasing the number of iterations.

4.4. Confusion matrices for classification

The confusion matrices presented in Figures 20 to 22 are used to correctly classify the 10 classes of bearing defects using each of the methods presented. Each matrix is constructed from a preferred class (y-pred) and a real class (y-true). For each method (CONV1D, LSTM and CONV1D+LSTM), several data elements of a row class were classified to their corresponding column class.

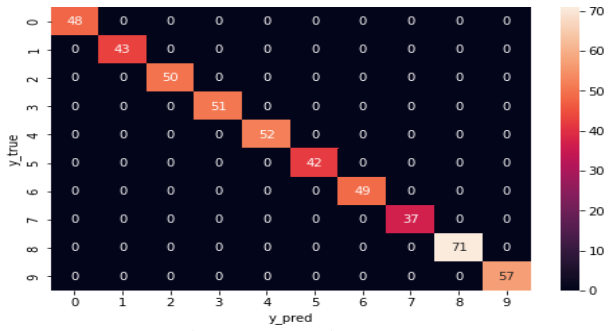

Fig. 20: Confusion Matrices for CONV1D Networks.

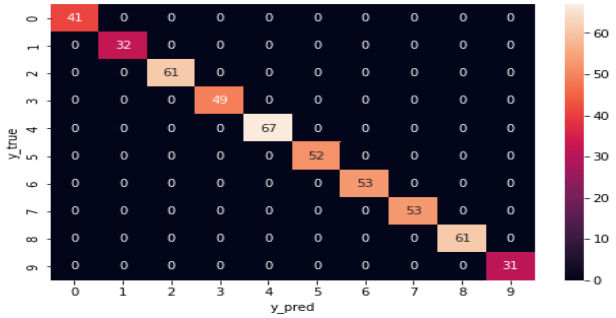

Fig. 21: Confusion Matrices for LSTM Networks.

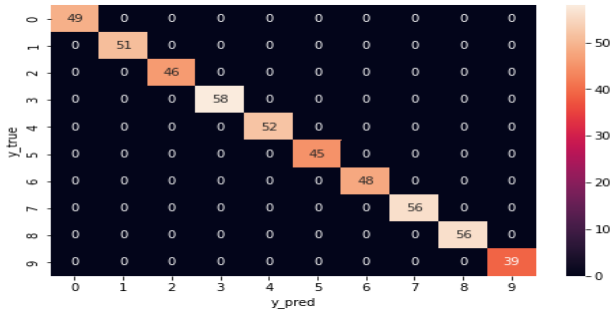

Fig. 22: Confusion Matrices for CNN+LSTM Networks.

These matrices for each method show the number of well classified samples for each class of defects after the models have been trained and tested with the different data samples in order to predict the best possible diagnosis.

5. Conclusion and outlook

The main objective of this paper was to methodically present a model of a diagnostic system for studying and assessing the various faults on an SKF bearing. To do this, we used a combination of layers (1D convolution) and enhanced LSTM memory layers. For the RNC, we used a CRWU online dataset on SKF bearings, which had four layers according to its structure. We accompanied this network with LSTM layers that used the temporal method of vibration analysis through the 10 signals of the 10 bearing states. From the accuracy rate of the training of the combination of the two models, we conclude that the result is better with the two models if we increase the number of iterations but with a longer training and testing time than when we train the methods (1D convolution) and the improved LSTM memories alone. In order to obtain a sizeable diagnosis, it was judicious to construct the confusion matrices that would group the data samples and classify them according to their volume in order to facilitate training and testing.

The method combining one-dimensional convolutional neural networks and improved LSTM memories for the diagnosis of bearing faults using CWRU bearing data sets and vibration signal samples produced satisfactory results with regard to the model implemented. The experimental results demonstrate and validate the feasibility and performance of the improved CNN1D +LSTM classifier for bearing diagnosis. This proposed model improves the data training accuracy beyond 96.6% with its Deep Learning algorithm significantly better than models with conventional algorithms. The classification results show that the model obtained by the improved CNN1D+LSTM can train a larger volume of data.

In our further research, we will continue to combine more than two methods, such as CNN+RNN+LSTM and many others, in order to seek the lowest margin of error tending towards zero and the highest possible percentage accuracy approaching 100% at the end of the training process for our model. The aim is to make diagnosis more reliable and of higher quality.

Acknowledgement

The authors would like to thank the anonymous reviewers for their time and effort. Their constructive comments and helpful suggestions helped us to clarify the main paper's research contributions and improve its quality.

References

[1] Gu, K., Zhang, Y., Liu, X., Li, H., & Ren, M. (2021). DWTLSTM-Based Fault Diagnosis of Rolling Bearings with Multi-Sensors. Electronics, 10 (7), 2076. https://doi.org/10.3390/electronics10172076.

[2] Oh, S., Han, S., & Jeong, J. (2021). Multi-scale convolutional recurrent neural network for bearing fault detection in noisy manufacturing environments. Applied Sciences, 11(9), 3963. https://doi.org/10.3390/app11093963.

[3] Zhao, Z., Xu, Q., & Jia, M. (2016). Improved shuffled frog leaping algorithm-based BP neural network and its application in bearing early fault diagnosis. Neural Computing and Applications, 27, 375-385. https://doi.org/10.1007/s00521-015-1850-y.

[4] Khorram, A., Khalooei, M., & Rezghi, M. (2021). End-to-end CNN+ LSTM deep learning approach for bearing fault diagnosis. Applied Intelligence, 51(2), 736-751. https://doi.org/10.1007/s10489-020-01859-1.

[5] Qiao, M., Yan, S., Tang, X., & Xu, C. (2020). Deep convolutional and LSTM recurrent neural networks for rolling bearing fault diagnosis under strong noises and variable loads. Ieee Access, 8, 66257-66269. https://doi.org/10.1109/ACCESS.2020.2985617.

[6] Slavič, J., Brković, A., & Boltežar, M. (2011). Typical bearing-fault rating using force measurements: application to real data. Journal of Vibration and Control, 17(14), 2164-2174. https://doi.org/10.1177/1077546311399949.

[7] Amar Chiter. (2001). Detection and diagnosis of bearing faults: contribution to the maintenance of rotating machines. Master's thesis in optics and accuracy mechanics». UFAS.

[8] Schmidhuber, J. (2015). Deep learning in neural networks: An overview. Neural networks, 61, 85-117. https://doi.org/10.1016/j.neunet.2014.09.003.
[9] Pan, H., He, X., Tang, S., & Meng, F. (2018). An improved bearing fault diagnosis method using one-dimensional CNN and LSTM. Journal of Mechanical Engineering/Strojniški Vestnik, 64.
[10] Fukushima, K. (1980). Neocognitron: A self-organizing neural network model for a mechanism of pattern recognition unaffected by shift in position. Biological cybernetics, 36(4), 193-202. https://doi.org/10.1007/BF00344251.
[11] Wen, L., Li, X., Gao, L., & Zhang, Y. (2017). A new convolutional neural network-based data-driven fault diagnosis method. IEEE Transactions on Industrial Electronics, 65(7), 5990-5998. https://doi.org/10.1109/TIE.2017.2774777.
[12] Hochreiter, S., & Schmidhuber, J. (1997). Long short-term memory. Neural computation, 9(8), 1735-1780. https://doi.org/10.1162/neco.1997.9.8.1735.
[13] Huang, H., & Baddour, N. (2018). Bearing vibration data collected under time-varying rotational speed conditions. Data in brief, 21, 1745-1749. https://doi.org/10.1016/j.dib.2018.11.019.